Available online at www.sciencedirect.com
SCIENCE DIRECT
Carbohydrate Polymers 61 (2005) 103–110
Carbohydrate Polymers
www.elsevier.com/locate/carbpol

Drying morphologies and related wetting and impregnation behaviours of 'sodium-alginate/urea' inkjet printing thickeners

A. Baffoun[a,b], P. Viallier[b], D. Dupuis[b], H. Haidara[a,*]

[a]*Institut de Chimie des Surfaces et Interfaces, ICSI-CNRS, 15 rue Jean Starcky-B.P. 2488, 68057 Mulhouse Cedex, France*
[b]*Laboratoire de Physique des Matériaux Textiles, ENSITM, 11 rue Alfred Werner, 68093 Mulhouse Cedex, France*

Received 12 August 2004; revised 27 February 2005; accepted 8 March 2005
Available online 17 May 2005

Abstract

The drying conditions of wet processed polymers, in general, and of high water-sorbing polymers, in particular are known to strongly affect their physical properties. We here investigate these drying morphologies for 'alginate–urea' compounds which are widely used as functional coatings in textile. We show how drastically the wetting and impregnation behaviours of the coating are affected by the drying conditions and resulting crystallisation morphologies. Furthermore, the contact of water drops during wetting measurements was found to induce morphological reconstruction through 'swelling/re-drying' process, leading to the formation of large and highly anisotropic needle crystals in coatings that were initially amorphous. Beyond the studied 'alginate–urea' system, these results provide insights into the evaporation-driven crystallization of solvent-processed compounded materials.

Keywords: 'Alginate–urea' compound; Inkjet printing thickener; Morphologies; Wetting; Impregnation

1. Introduction

Alginate belongs to the wide class of highly swellable polyssacharide polymers that form hydrocolloid suspensions in water (Narayani, Gita, & Amarnathan, 2000; Tolstoguzov, 2004). While the constitutive alginic acid chains of this polysaccharide are insoluble in water, their monovalent salts (Na^+, K^+, NH_4^+) actually termed alginate are soluble. One of the outstanding property of alginate is its ability to form heat-stable and irreversible hydrogels at room temperature when processed with divalent cross-linkers (calcium chloride solution, especially) (Hair, Chandy, & Sharama, 1996; Kim, Yoon, Lee, Lee, & Kim, 2003; Wang et al., 2003). Widely known and used for long time in food and make-up industries (McCormick, 2001), alginate has received over recent years a great deal of interest as an alternative candidate for biological and clinical applications, as well as functional coatings (thickener) in ink-jet printing of textile fabrics (El-Molla & El-Sayad, 2001; Gutjahr & Koch, 1994; Hair et al., 1996; Kim et al., 2003; Knill et al., 2004; McConnell, Jarman-Smith, Stewart, & Chaudhuri, 2003; Narayani et al., 2000; Schneider & Sostar-Turk, 2003; Wang et al., 2003; Zohar-Perez, Chet, & Nussinovitch, 2004). For the latter application where the coating is intended to 'temporary' entrap impacting droplets and to control their spreading and diffusion towards the fabrics, *alginate* is currently compounded with *urea*. Therefore, the morphological structures resulting from the processing conditions (drying) of these 'alginate–urea' thickeners are of crucial importance as regards the competing phenomena of wetting, diffusion and imbibition which critically control the whole inkjet printing process. If an abundant literature exists on the dynamics of impacting drops (Emmel & Hersch, 2000; Mourougou-Candoni, Prunet-Foch, Legay, Vignes-Adler, & Wong, 1997; Prunet-Foch, Legay, Vignes-Adler, & Delmotte, 1998; Zhang & Basaran, 1997), investigations dealing with the drying morphologies of 'alginate–urea' coatings (Vidal, Lekka, Kulik, & Wandrey, 2001; Zohar-Perez et al., 2004), in relation with the presence of *the highly crystallisable urea compound* (Boek, Feil, & Briels, 1991; Docherty, Roberts, Saunders, Black, & Davey, 1993), on

* Corresponding author. Tel.: +33 3 89 60 88 39; fax: +33 3 89 60 87 99.
E-mail address: hamidou.haidara@uha.fr (H. Haidara).

0144-8617/$ - see front matter © 2005 Published by Elsevier Ltd.
doi:10.1016/j.carbpol.2005.03.018

the one hand, and the way these affect their functional properties, on the other hand, are very rare. In the following, we address this topic which covers, well beyond the 'alginate–urea' binary system, the morphology-dependent properties of most solvent-processed polymer coatings.

2. Experimental section

For these experiments, a standard sol recipe mostly applied in fabrics industries for the elaboration of 'alginate–urea' thickener pastes was used (Provost, 1992; Gutjahr & Koch, 1994). This formulation basically consists of a mixture of sodium alginate (Na-alginate), water, urea and sodium bicarbonate, in the proportion (in wt.%) of 2.5, 85, 10 and 2.5, respectively. The medium viscosity Na-alginate (CHT ALGINAT SMT) was from CHT, R. BEITLICH GmbH, Germany, and the urea $(NH_2)_2CO$, and sodium bicarbonate were from Prolabo. Both compounds were used as received. Deionised and twice distilled water was used for all preparations and experiments. The role of urea is to provide the thickener with hydrogen-binding species that can retain some water and fix the dye molecules within the coating, during and after the printing step. The locally entrapped dyes (ink droplets) are released and allowed to diffuse towards textile fibres during a final vapour-swelling step. The thickener solution was prepared as follows. First, water (85 g/100) was introduced in a glassware and warmed up to 70 °C. Urea that actually constitutes the major component was then added under mechanical stirring, followed by the sodium alginate (powder), which was progressively poured in the mixture. Sodium carbonate was added at the end, while maintaining the stirring for ~30 min. The shear viscosity η of the resulting formulation was measured and found to well compare with quoted values (Schneider & Sostar-Turk, 2003), ranging from 4.4 to 6.4 Pa s, for shear rate values ranging from 10 to 1 s^{-1}, respectively. The equilibrium contact angle of the formulation was measured on clean hydrophilic glass and found to be ~5°. This quite low value was obtained within ~5 min spreading, starting from an initial value of ~20°. Three coatings of thicknesses 70 μm ± 10, 30 ± 5 and 13 μm ± 3 were elaborated by spin casting the required volume of the solution on 2.5 × 3 cm^2 glass slides, typically for 30 s at an angular velocity of 2000 rpm. Before spin-coating, the glass slides were treated in piranha solution (3:7 v/v of 30% H_2O_2 and H_2S0_4 mixture) (Mougin, Castelein, & Haidara, 2004), thoroughly rinsed with deionized and twice distilled water, and then dried under nitrogen. This treatment is aimed at producing clean hydrophilic surfaces. Five drying conditions of the coatings were used: (1) the air drying in ambient laboratory environment (22 °C, 30% RH), which for the studied film thickenesses takes ~15 min for completion and, (2) the oven drying at 40, 60, 70 and 110 °C for 2 min, the latter reproducing roughly the conditions applied in textiles. Finally, the residual amount of water in the dried coatings were determined for the 70 μm thick film by thermo-gravimetric measurements, leading for the two extreme drying conditions, ambient and oven(110 °C, 2 min), to 56 and 48.5 wt%, respectively.

The morphology-dependent wetting studies (spreading, imbibition, structural changes of the coating) were performed using water droplets, the time evolution of which were captured with a video-camera (CCD) recording device, and compared to a reference system represented by the 'virgin glass/drop' couple. When necessary, an optical microscope coupled to a CCD was used for the observation of the fine morphological structures.

3. Results and discussion

The representative optical micrographs of the drying morphologies, which were found not to depend on the thickness of the coating in the investigated range are given, in Fig. 1, for the thicker film. Whereas the oven drying morphology is essentially uniform and homogeneous at this micrometer scale, the one resulting from ambient condition is characterized by the growth of large and highly anisotropic crystalline domains, which are made of inter-penetrated single fibril crystals. We have observed (see two last figures of the paper) that these needle-like structures which are in all aspects similar to urea crystals grown from evaporating polar solvents (Boek et al., 1991; Docherty et al., 1993), essentially nucleate from the borders, as expected for heterogeneous nucleation (Giegé & Ducruix, 1992), covering in about 15 min the entire sample as the drying proceeds inwards. Furthermore, its seems that the drying and urea crystallization is accompanied by a segregation during which the urea phase separates from the residual components (alginate + sodium bicarbonate) which form a thin film with dendrite-like domains underneath the fibrils (crystals), as illustrated by the magnified 'inter-fibrillar' zone in the insert of Fig. 1d. This hypothesis was further supported by the complementary experiments we did with urea-free solution, the drying morphology of which (not shown here) was exclusively made of the same 'thin film with dendrite-like domains' observed in the 'inter-fibrillar' zone shown in the insert of Fig. 1d. The morphological difference arising from the above two drying conditions seems to suggest the critical role the extraction kinetics (Anit, Cyriac, & Ittyachen, 2001), on one hand, and the 'equilibrium' residual water amount, on the other hand, may play in determining the ultimate morphology of the coating. For this high water-sorbing 'alginate–urea' compound, this residual water amount which we showed to be higher in the ambient dried coatings is determined by the vapour pressure ($P^*_{v,T}$) of the structural water entrapped in the coating, at temperature T. If ε_0 and ε^*, stand for the vaporization energy of the pure, and of structural water entrapped in the network of ionic and/or H-bonds junctions of the water-based viscous alginate sol, respectively, one

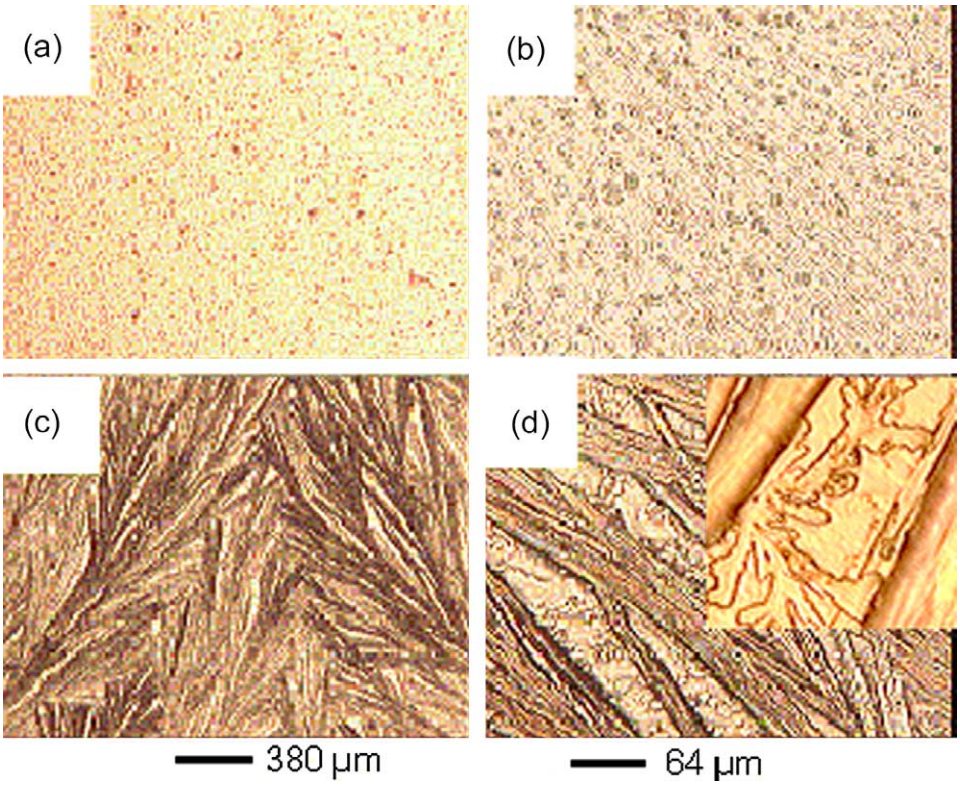

Fig. 1. Optical micrographs showing the representative morphologies resulting from the two extreme drying conditions; (a) and (b) oven-dried (110 °C, 2 min) and, (c) and (d) ambient-dried (22 °C, 30% RH) with the inset showing the magnified view of a 'inter-fibrillar' zone.

may expect both the vapour pressure achieved during the drying ($P^*_{v,T}$) and the amount of water extracted from the coating/unit time (rate) to follow an Arrhenius-type equation, $(P^*_{v,T}/P^0_{v,T}) \sim \exp[-(\varepsilon^* - \varepsilon_0)/kT]$. In this equation, $P^0_{v,T}$ and $(\varepsilon^* - \varepsilon_0) = \varepsilon_A (>0)$, represent, respectively, the vapour pressure of the 'free' drop water, and the excess energy cost for the extraction of the water entrapped in the polymer network, with respect to 'free' water in the drop, and k is the Boltzmann constant (1.38×10^{-23} J K^{-1}). The amount of residual equilibrium water in the dried coating is thus expected to be higher at ambient temperature, in agreement with our thermogravimetric measurements (see Section 2). The role of the extraction kinetics in the morphological differentiation is rather dynamical, since it determines both the nucleation density (Anit et al., 2001) and growth rate in the drying material through the time-dependent events of molecular transport and collective relaxation. In ambient conditions, the extraction kinetics allows enough time for urea molecules to diffuse through an alginate network that remains 'swelled' and more mobile (chain mobility) over a large timescale, whereas this chain mobility and urea diffusion are hindered by the faster drying kinetic and resulting rapid collapse of the hydrocolloid network at higher temperature. In order to bring further evidence towards these results and related phenomenology, we developed complementary experiments aimed, (1) at adjusting the morphology of the coating in between the ambient and oven (110 °C, 2 min) drying morphologies and, (2) at identifying the plausible transition temperature between these two morphological structures. This was done by performing the drying experiment at three intermediate temperatures, 40, 60, 70 °C in oven. These intermediate drying morphologies are shown in Fig. 2.

As compared to the two 'extreme' morphological types shown in Fig. 1, both the fine morphological details (size and length of needles and domains) and large scale topological feature of the coating were found to be sensitive to the drying temperature (kinetics). Furthermore, a morphological transition located around 65 °C was evidenced between the large fibrillar crystals structure and the macroscopically homogeneous one that is actually composed of much smaller crystals, as we observed by Atomic Force Microscopy (picture not shown here). In term of crystallization thermodynamics, this temperature dependence of crystallization morphology is related to the thermally nucleation rate, R_n, expressed by a Arrhenius-type relation (Giegé & Ducruix, 1992; Hoffman & Miller, 1997), $R_n \sim C_s(kT/h)\exp(-\Delta G_n/kT)$, where ΔG_n represents the activation free energy of germination, which normally involves a chain diffusion term to the nucleus (additional energy barrier). The prefactor is the product of the saturation concentration (at temperature T) by a frequency term (kT/h), where h is the Planck constant (6.62×10^{-34} J s). Because both the coatings shown in Figs. 1 and 2 have identical

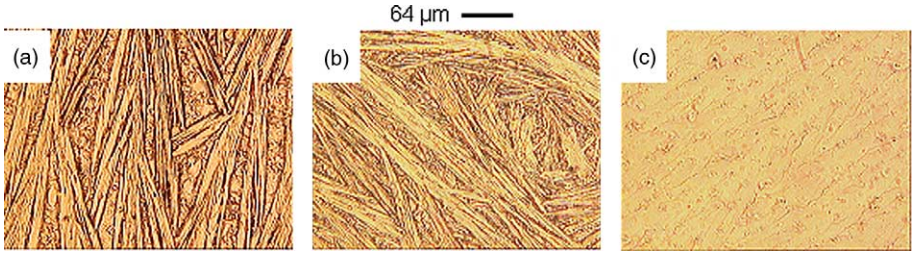

Fig. 2. Structural evolution of the drying morphology with temperature; (a) oven (40°, 4 min), (b) oven (60°, 2 min) and, (c) oven (70°, 2 min). The transition between the morphologies typical of ambient and 'high' temperature drying is roughly located around 65 °C.

nominal concentration C_s, one expects the nucleation rate R_n to be dominated at first order by the exponent, $(-\Delta G_n/kT)$, increasing with the drying temperature from $\sim$293 K (ambient) to 383 K (maximum oven-drying temperature herein tested). Related to the nucleation rate R_n, it is nucleation density, $\sim R_n\tau_c$, where τ_c represents the time to the completion of the *nucleation* process (*not growth*!), which definitely controls the temperature-dependent drying morphologies (crystals density and fineness). And the higher R_n (actually $R_n\tau_c$), the smaller the crystals, and the more homogeneous the morphology will appear at the macroscopic scale, and vice-versa. One thus expects the drying morphologies to range, as shown in Figs. 1 and 2, from large crystal domains at low R_n (from T_{amb} to 60 °C), to very small crystals at high R_n ($T \geq 70$ °C), with a transition located around 65 °C. Although the intimate growth mechanisms of the urea needle-crystals, and especially, their interplay with the surrounding alginate chains remain somewhat unclear at this point, our results show that there are at least two critical parameters that feature the ultimate drying morphology of these 'alginate–urea' compounds. These are the extraction kinetic of water (solvent) from the swelled network, on the one hand, and the residual amount of structural water, on the other hand. Finally, it is interesting to note here that whereas the physical properties of the mixed 'alginate–urea' solution mostly reflects those of the alginate compound (high swelling and high viscosity at relatively low concentration), the drying morphology is, on the other hand completely dominated by the crystallisation behaviour of the urea compound (Boek et al., 1991; Docherty et al., 1993). As regards the functional properties of these coatings and, in particular, those of wetting, imbibition and diffusion required for both ink-jet printing and other applications, one can reasonably expect the two characteristic drying morphologies to lead to singularly different behaviours. In the following, these wetting-impregnation properties of the two morphological structures were studied under ambient (22 °C, 30% RH), with respect to the virgin glass, using 5 µl water drops. The 'drop/virgin glass' couple which behaviour is exclusively dominated by evaporation (after the early spreading) provides the reference system for analysing the impregnation of liquid into the coating. These wetting experiments are aimed here, at essentially demonstrating and highlighting, the morphology dependence and competition between spreading and imbibition, which are crucial functional properties of this increasingly used coating material. In Fig. 3 are represented few panels illustrating the time evolution of the drop profile on the two extreme characteristic drying morphologies.

A side view of the drop has been deliberately incorporated in Fig. 3 (panel f, ambient-dried coating) to underscore the limitation of the common practice that often

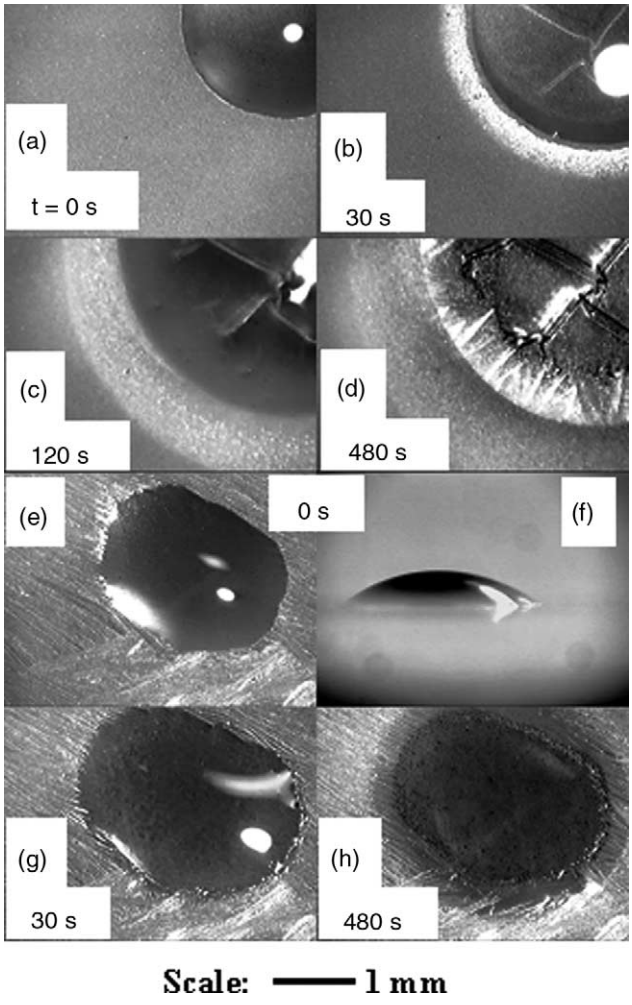

Fig. 3. Panels (video) showing the top-view of the drop at different times on the thicker coating, for the two extreme drying conditions, (a–d) oven (110°, 2 min), and (e–h) ambient (22 °C, 30% RH).

consists in assessing the wetting of a substrate uniquely from side-view pictures and contact angles. In principle, if such data are consistent for substrates that are homogeneous at scales much smaller than the size of the drop [oven-dried (110 °C, 2 min)], they clearly appear insufficient to account for the non uniform wetting on substrates presenting complex surface morphologies (anisotropy, fractals, etc.), as shown by the elliptical drop profile on ambient dried coatings. Further evidence towards this is provided by the formation of a diffusion front ahead of the drop (in the coating), which can here be observed and studied only in top view configuration. Although wetting phenomena were more uniform on oven (110 °C, 2 min) dried coatings (*axi-symmetrical drop profile and diffusion front*), the *too high impregnation rate and magnitude* did not allow to reliably measure the time-decrease of the drop height, except on the lowest 'oven-dried' coating thickness, which has the smaller sink volume. We therefore studied the thickness dependence of the wetting kinetics only for the ambient-dried coating, which present enough slow kinetics. These wetting kinetics are plotted in Fig. 4 in adimensional drop height (h_t/h_0), and diameter (D_t/D_0), for which the average of the longer and shorter sizes of the contact area was considered. Of course, when asymmetric drop profile occurs (Fig. 3), these 'height–diameter' pairs are no longer relevant for standard surface energetic analyses (Young law, Wenzel and Cassie-Baxter relations), which both assume a priori homogeneous wetting with quasi-equilibrium contact angles (De Coning, Dobrovolny, Miracle-Solé, & Ruiz, 2004). Nevertheless, when considered for a set of coating exhibiting identical morphological anisotropy and wetting asymmetry, these 'height–diameter' pairs become pertinent for comparing their spreading and imbibition behaviours. This is what is mainly done here, using different thicknesses of the same needle-like morphology of ambient-dried coatings.

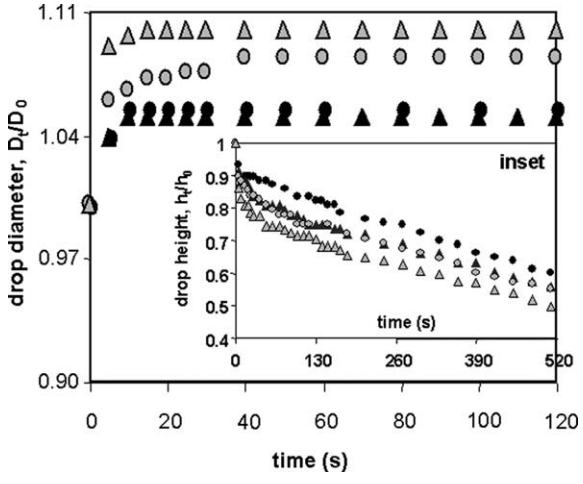

Fig. 4. Wetting kinetics as given by the time-variation of the drop diameter and height on the virgin glass (●) and ambient-dried coatings of 71 (▲), 30 (◎) and, 13 μm (△).

A priori, these plots display the standard profile expected for the time-evolution of simple liquid drops of low viscosity, under good wetting conditions (high spreading rate and extent followed by the late stage plateau). In fact, the unique distinctive features in these plots that are specific of the coatings are the slopes and magnitudes of h_t and D_t, with respect to the virgin glass. These slopes and magnitudes here account for the liquid impregnation into the coating and its thickness dependence. From the comparison of these quantities, it can be seen that the spreading rate on the ambient-dried coatings, though much lower as compared to oven-dried coatings, still remains slightly higher than on virgin glass. This also is the case for the extent of the spreading at contact line 'stabilization', except for the thicker coating which has a equilibrium spreading size comparable to the virgin glass. Most interestingly, this extent D_t was found to increase slightly (but in a reproducible way) as the inverse of the thickness of the coating, suggesting some early contribution of the impregnation which can be expected to increase with the size of the imbibition sink (thickness). Therefore, the thicker the coating, the higher the amount of water taken from the drop in the early stage and, the lower the residual drop volume that contributes to the spreading. The magnitude of the lowering in the drop height h_t (inset plot) which also increases, from the glass substrate, as the inverse of the thickness of the coating well supports this combined influence of spreading and impregnation on the wetting kinetics of the coatings in the early stage (up to 60 s). After the stabilisation of the contact area D_t, typically after the early 100 s, both the coatings and glass substrate behave similarly (comparable slopes). Surprisingly, the drop height still remains measurable on both coatings over sufficiently large timescale, in spite of this combined influence of spreading and impregnation. This certainly constitutes one of the interesting morphology-related feature of these wetting kinetics, which can be accounted for by the early impregnation, and the strong resulting re-dilution and swelling of the coating beneath the drop. As already discussed above, the rate of vaporisation (extraction) of the water entrapped in this swelled polymer network was shown to be much lower, as compared to free water drops on glass substrate. The vertical expansion of the swelled polymer network in the wetting spot may thus lead to the formation of local bumps, whose size and time-decrease can be measured on durations comparable to that of 'free' water droplets on glass. The most impacting result of these morphology-dependent wetting studies as regards the structural changes that can take place beneath a contacting fluid (and more generally in confined interfaces) is probably the drastic morphological transition which results locally from the re-drying of the swelled coating in ambient conditions. These structural changes that are identically observed on both oven and ambient-dried coatings are shown in Fig. 5a for oven (110 °C, 2 min)-dried films, which also provide the most visual contrast between the initial

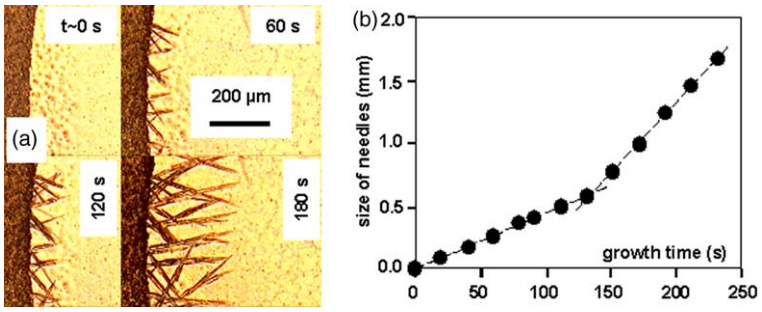

Fig. 5. Re-drying of the swelled wetting spot in ambient conditions. (a) Video-microscopy images showing the early growth of the needle crystals from the boundary of the virgin/swelled coating, and (b) growth kinetic of the crystals (length vs. time) plotted from the end (~150–300 s) of the early emergence stage shown in (a). Note the roughening of the swelled close to the boundary that precedes the growth of needles.

morphology and the one resulting from the re-drying of the swelled spot. At the difference of the heterogeneously nucleated dense fibrous crystals that characterise the ambient drying morphology of freshly spin-coated sols, the needle crystals arising from the re-drying of the swelled spot rather nucleate from the 'unswelled' boundary crystals (secondary nucleation process), and form a less dense structure at completion. These morphological differences actually reflect two crystallization kinetics, which were found to differ significantly for the freshly spin-coated sol, on one hand, and the swelled-spot, on the other hand. The selected panels of Figs. 5a and 6a, which represent the time-growth of the structures in the swelled-spot, and in the freshly spin-coated sol, well account for these differences in the crystallization (drying) kinetics and resulting morphologies (density and fineness of crystals). At the difference of the morphological transition shown in Fig. 2 for freshly-coated samples, which were identical in all respects, except for the drying temperature, the temperature-dependence of the nucleation rate R_n cannot be evoked here for the morphological difference between the 'swelled-spot' and the freshly-coated sol, both coatings being dried at the ambient temperature. On the other hand, both the residual water content and the nucleation mode of the re-drying 'swelled coating' differ from those of the freshly coated sol. In particular, one may expect the lower amount of water in the 'swelled coating' to significantly hinder the diffusion (solvent-mediated transport) of urea molecules through the swelled network, towards the nuclei and growing crystals, as compared to the freshly spin-coated sol. This increased diffusion barrier that enters the activation free energy (ΔG_n), thus leads to an effective lowering of the nucleation rate and density, as given by $R_n \sim \exp(-\Delta G_n/kT)$, and discussed above. It thus seems that the consideration of the sole phenomenological dependence of the activation energy, and hence of the crystallization rate on the molecular diffusion, allows to reasonably account for the observed differences in the crystallization kinetics and resulting drying morphologies, between the 'swelled coating', and the freshly spin-coated sol. We characterised the growth kinetic of the fibrous crystals by following the time-evolution of their size (length), on both freshly spin-coated samples, and inside the wetting spot. These kinetics, which are typical of all ambient-dried coatings (either freshly cast or re-swelled) are plotted in Figs. 5b and 6b. These results show that the fibrils grow inside the swelled spot following two regimes, which both can be fitted linearly. In the early stage, a low growth rate is observed, followed in the late stage by a much faster growth kinetic. On freshly spin-coated samples, the fibrils essentially grow linearly, with a rate about two orders of magnitude higher than the average one measured inside the swelled spot.

It is clear that this is not very usual in standard wetting experiments to track and characterize these morphological modifications that can drastically affect the overall interface

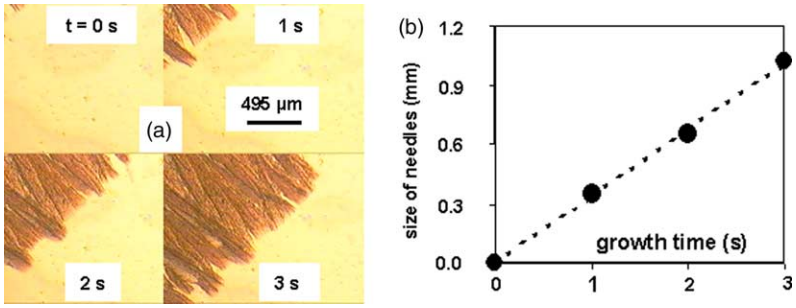

Fig. 6. Drying of freshly spin-coated sol in ambient conditions and growth kinetic of the dense needle crystals, illustrated in (a), by selected video-microscopy panels, and in (b), by the time-dependence of the length of the needle crystals.

and bulk physico-chemical properties of the coating. As regards ink-jet printing processes, these studies show that the drying mode (typically above 100 °C) generally applied in textile from rough empirical considerations, actually produces the optimal morphology for the uniform *spreading-diffusion and impregnation* of the droplets, and hopefully their diffusion through the coating, towards the fabrics. Well beyond the investigated 'alginate–urea' system, these results illustrate the way the whole morphology and properties of a multi-component material can be entirely determined by a unique constituent. They also show how profound structural changes that may not be a priori expected can take place in confined interfaces and affect the ultimate behaviour of a system. If interface phenomena involving such systems are analysed from their initial properties or from properties determined from non reactive probes, it is highly probable that these analyses may not adequately account for the actual behaviour of the system, unless these possible modifications are assumed or investigated. The most illustrative cases of such complex problem are generally encountered in solvent-processed polymer coatings, and especially, in solvent-assisted formation of polymer adhesive joints (Brown, 2000).

4. Conclusion

We studied the drying morphologies of 'alginate–urea' compounds that are currently used, among many other applications, as thickeners for inkjet printing of textiles, and showed how these morphologies crucially affect their wetting and impregnation behaviours. The two characteristic morphologies which result from the ambient and oven (highest temperature) drying were also found to exhibit two wetting and impregnation behaviours in between which the intermediate morphologies gradually evolve. Furthermore, morphological restructuring of the coating beneath the contacting drop (water), through swelling and 're-drying' cycle was observed under ambient conditions, and found to lead to the formation crystalline structures similar to those resulting from the drying of freshly coated films in ambient conditions. As regards the increasing applications of these alginate-based compounds, especially as thickeners in ink-jet printing of fabrics, these studies may provide some useful key routes towards the optimisation of their morphology-dependent wetting, impregnation, adsorption and diffusion properties.

Acknowledgements

The authors would like to think S. Gautier for his technical help with thermogravimetry measurements.

References

Anit, E., Cyriac, J., & Ittyachen, M. A. (2001). Growth and micro-topographical studies of gel grown cholesterol crystals. *Bulletin of Materials Science*, *24*(4), 431–434.

Boek, E. S., Feil, D., & Briels, W. J. (1991). From wave function to crystal morphology: Application to urea and alpha-glycine. *Journal of Crystal Growth*, *114*, 389–410.

Brown, H. R. (2000). Adhesion between polymers and other substances—A review of bonding mechanisms, systems and testing. *Materials Forum*, *24*, 49–58.

De Coning, J., Dobrovolny, C., Miracle-Solé, S., & Ruiz, J. (2004). Wetting of heterogeneous surfaces at the mesoscale. *Journal of Statistical Physics*, *114*, 575–604.

Docherty, R., Roberts, K. J., Saunders, V., Black, S., & Davey, R. J. (1993). Theoretical analysis of the polar morphology and absolute polarity of crystalline urea. *Faraday Discussions*, *95*, 11–25.

El-Molla, M. M., & El-Sayad, H. S. (2001). Rheological behaviour of sodium alginate solutions with added divalent metal salts and their use as thickeners in cotton printing with reactive dyes. *Advances in Polymer Technology*, *20*, 58–71.

Emmel, P., & Hersch, R. D. (2000). Exploring ink spreading. In *Proceedings of the 8th IS&T/SID Color Imaging Conference: Color Science and Engineering, Scottsdale, Arizona, November 7–10* (pp. 335–341).

Giegé, R., & Ducruix, A. (1992). An introduction to the crystallogenesis of biological macromolecules. In A. Ducruix, & R. Giegé (Eds.), *Crystallization of nucleic acids and proteins: A practical approach*2nd ed.. Oxford: Oxford University Press.

Gutjahr, H., & Koch, R. R. (1994). Direct print coloration. In Leslie W.C. Miles (Ed.), *Textile printing*2nd ed. (pp. 139–195). Oxford, Society of Dyers and Colourists: The Alden Press, 139–195.

Hair, P. R., Chandy, T., & Sharama, C. P. (1996). Chitosan/calcium-alginate beads for oral delivery of insulin. *Journal of Applied Polymer Science*, *59*, 1795–1801.

Hoffman, J. D., & Miller, L. R. (1997). Kinetics of crystallization from the melt and chain folding in polyethylene fractions revisited: Theory and experiment. *Polymer*, *38*(13), 3151.

Kim, S. J., Yoon, S. G., Lee, S. M., Lee, J. H., & Kim, S. I. (2003). Characteristics of electrical responsive alginate/poly(diallyldimethylammonium chloride) IPN hydrogel in HCl solutions. *Sensors and Actuators B*, *96*, 1–5.

Knill, C. J., Kennedy, J. F., Mistry, J., Miraftab, M., Smart, G., Groocock, M. R., et al. (2004). Alginate fibres modified with unhydrolysed and hydrolysed chitosans for wound dressings. *Carbohydrate Polymers*, *55*, 65–76.

McConnell, K., Jarman-Smith, M. L., Stewart, K., & Chaudhuri, J. B. (2003). Culture of meniscal chondrocytes on alginate hydrogel matrices. *European Cells and Materials*, *6*(2), 22.

McCormick, E. (2001). Alginates-Lifecasters' gold. *Art Casting Journal* .

Mougin, K., Castelein, G., & Haidara, H. (2004). *Tribology Letter*, *17*, 11–17 (Caution: Piranha solution reacts violently with organic compounds and must be handled with care).

Mourougou-Candoni, N., Prunet-Foch, B., Legay, F., Vignes-Adler, M., & Wong, K. (1997). Influence of dynamic surface tension on the spreading of surfactant solutions droplets impacting onto a low-surface-energy solid substrate. *Journal of Colloid and Interface Science*, *192*, 129–141.

Narayani, R., Gita, V. B., & Amarnathan, T. (2000). Preparation and evaluation of alginate films for periodontal drug delivery. *Trends in Biomaterials and Artificial Organs*, *14*, 1–4.

Provost, J. R. (1992). Effluent improvement by source reduction of chemicals used in textile printing. *Journal of the Society of Dyers and Colourists*, *108*, 260–264.

Prunet-Foch, B., Legay, F., Vignes-Adler, M., & Delmotte, C. (1998). Impacting emulsion drop on a steel plate: Influence of the solid substrate. *Journal of Colloid and Interface Science*, *199*, 151–168.

Schneider, R., & Sostar-Turk, S. (2003). Good quality printing with reactive dyes using guar gum and biodegradable additives. *Dyes and Pigments*, *57*, 7–14.

Tolstoguzov, V. (2004). Why are polysaccharides necessary? *Food Hydrocolloids*, *18*, 873–877.

Vidal, D. S., Lekka, M., Kulik, A. J., & Wandrey, C. (2001). Surface characterization of hydrogel-based microspheres. *European Cells and Materials*, *6*(1), 81.

Wang, L., Shelton, R. M., Cooper, P. R., Lawson, M., Triffitt, J. T., & Barralet, J. E. (2003). Evaluation of sodium alginate for bone marrow cell tissue engineering. *Biomaterials*, *24*, 3475–3481.

Zhang, X., & Basaran, O. A. (1997). Dynamic surface tension effects in impact of a drop with a solid surface. *Journal of Colloid and Interface Science*, *187*, 166–178.

Zohar-Perez, C., Chet, I., & Nussinovitch, A. (2004). Irregular textural features of dried alginate-filler beads. *Food Hydrocolloids*, *18*, 249–258.